crystals

MDPI

Article

Crystallization of Calcium Carbonate in Alginate and Xanthan Hydrogels

Cleo Kosanović [1], Simona Fermani [2], Giuseppe Falini [2,*] and Damir Kralj [3,*]

[1] Meteorological and Hydrological Service, Air Quality Division, Grič 3, HR-10000 Zagreb, Croatia; kosanovic@cirus.dhz.hr

[2] Dipartimento di Chimica "Giacomo Ciamician", Alma Mater Studiorum—Università di Bologna, via Selmi 2, 40126 Bologna, Italy; simona.fermani@unibo.it

[3] Ruđer Bošković Institute, P.O. Box 180, HR-10002 Zagreb, Croatia

* Correspondence: giuseppe.falini@unibo.it (G.F.); kralj@irb.hr (D.K.); Tel.: +39-051-209-9484 (G.F.); +385-1-468-0207 (D.K.)

Academic Editor: Linda Pastero

Received: 20 September 2017; Accepted: 27 November 2017; Published: 30 November 2017

Abstract: Calcium carbonate polymorphs were crystallized in alginate and xanthan hydrogels in which a degree of entanglement was altered by the polysaccharide concentration. Both hydrogels contain functional groups (COOH and OH) attached at diverse proportions on saccharide units. In all systems, the precipitation process was initiated simultaneously with gelation, by the fast mixing of the calcium and carbonate solutions, which contain the polysaccharide molecules at respective concentrations. The initial supersaturation was adjusted to be relatively high in order to ensure the conditions suitable for nucleation of all $CaCO_3$ polymorphs and amorphous phase(s). In the model systems (no polysaccharide), a mixture of calcite, vaterite and amorphous calcium carbonate initially precipitated, but after short time only calcite remained. In the presence of xanthan hydrogels, precipitation of either, calcite single crystals, porous polyhedral aggregates, or calcite/vaterite mixtures were observed after five days of ageing, because of different degrees of gel entanglement. At the highest xanthan concentrations applied, the vaterite content was significantly higher. In the alginate hydrogels, calcite microcrystalline aggregates, rosette-like and/or stuck-like monocrystals and vaterite/calcite mixtures precipitated as well. Time resolved crystallization experiments performed in alginate hydrogels indicated the initial formation of a mixture of calcite, vaterite and amorphous calcium carbonate, which transformed to calcite after 24 h of ageing.

Keywords: calcium carbonate; crystallization; hydrogels; alginate; xanthan

1. Introduction

The formation of diverse calcium carbonate ($CaCO_3$) solid phases is one of the most investigated precipitation process among slightly soluble ionic salts. In this system, three polymorphs (vaterite, aragonite or calcite), two hydrates (monohydrocalcite, $CaCO_3 \cdot H_2O$ and ikaite, $CaCO_3 \cdot 6H_2O$) and amorphous calcium carbonate can precipitate. Therefore, their formation pathways provide suitable models for basic the investigation of mechanisms and kinetics of nucleation, crystal growth, dissolution and, particularly, transformation of precursor phases in aqueous solutions. In addition, $CaCO_3$ phases are extensively investigated because of their relevance in geological, technological and biological environments and systems [1–6].

The most important experimental parameters, which influence the precipitation of slightly soluble salts like $CaCO_3$ and their structural, chemical and morphological properties, are the initial supersaturation, temperature, presence of additives, pH and hydrodynamic conditions. Consequently, the traditional experimental protocols, like bulk precipitation, crystal seeding, constant composition or

continuous processes, are regularly applied for tuning the properties of the precipitate. Crystallization of slightly soluble salts in gelling environments is inspired by biomineralization of $CaCO_3$ in mollusks and corals, or calcium phosphates in enamel and bones and it has been recognized as an alternative strategy for synthesis of materials with desired features [7]. Hydrogels are multicomponent, solid-like systems built up by a three-dimensional network of interconnected (macro) molecular chains, with the interspace filled up with water and possibly electrolytes. The formation of gel-like structures and their physical and chemical properties are principally influenced by the concentration of the gelling molecules, temperature, pH and in some specific cases, type and concentration of counter and co-ions present in the system [7,8]. In such gelling systems, the critical parameters for precipitation are mostly determined by diffusivity and the local charge distribution (ionotropic effect) [9–11].

Biocompatible polysaccharide hydrogels have been recognized as suitable models for investigation of $CaCO_3$ precipitation (crystallization), particularly for clarifying the role of basic processes (nucleation, crystal growth, dissolution or aging) [7,10,12–14]. However, a more explicit connection between calcium carbonates and gels is related to their possible biomedical or pharmaceutical application. Thus, for example, a class of hybrid organic–inorganic drug delivery systems, constructed from porous micro particles in which active molecules are absorbed and coated with polymer multilayers has been described. In such systems, layer-by-layer adsorption of differently charged polyelectrolytes onto porous vaterite particles may form microcapsules with gel-like interior, after removing the mineral core [15–18]. Thus, size, polymorphic composition, surface texture and/or porosity, can influence their properties relevant for potential use as a drug delivery vehicles. A role of the above-mentioned parameters is intuitively understandable and can be correlated to the efficiency of delivery. However, control of the particles' shape is recognized as a future trend in preparation of drug delivery models, since it was described that anisotropic particles show higher intracellular transport [19–23].

In addition, within the field of tissue engineering, hydrogel composites with inorganic micro particles are intensively investigated as materials for bone regeneration. Since bones can be considered as a mineralized hydrogel made of collagen fibrils and calcium-deficient hydroxyapatite, a production of synthetic hydrogel–inorganic composites is supposed to mimic the nature [24–26]. In such systems, mineral phases increase the composites' bioactivity, surface roughness, mechanical properties, adhesion, proliferation and differentiation of bone-forming cells. Convenient inorganic phases used for hydrogels enrichment are calcium phosphates and bioactive glasses, but silica and $CaCO_3$ are considered as well. Typical experimental strategies for mineralization of respective hydrogels with $CaCO_3$ involved either, mixing of previously formed particles with sols before gelation (so called "internal gelation") [27–30], or their precipitation after gelation. Indeed, in the case of postponed formation of mineral particles, precipitating components have been delivered by different techniques. Thus for example, $CaCO_3$ precipitation has been initiated by alternating a soaking of poly(acrylic acid) grafted poly(ethylene) films into Ca^{2+} or CO_3^{2-} solutions. Similar protocols have been applied for agarose or chitosan gels [14,31–33]. A diffusion of one component (CO_2) into the agarose gel preloaded with Ca^{2+} and modified with self-assembled monolayer, has been investigated as a model of biomineralization of protein-based hydrogels. In such systems nucleation and growth were simultaneously controlled [34]. Double-diffusion of calcium and carbonate ions into the polyacrylamide hydrogels of different polymer content has been investigated and a correlation between morphology of precipitate and hydrogel concentration was found [35]. A similar experimental setup was also applied in the agarose hydrogel system in order to estimate the impact of porosity on the properties of mineral phase and to correlate it with supersaturation profile and presence of additives [36,37]. Besides the above-mentioned two-step protocols, simultaneous gel and $CaCO_3$ formation has also been described. Thus, stepwise addition of Na_2CO_3/alginate solution into $CaCl_2$ resulted in creation of appropriate composites and allowed the authors to recognize an active control of the gel matrix over the size and morphology of the obtained calcite crystals [13]. Similarly, simultaneous

$CaCO_3$ precipitation and gelling of carrageenan, accomplished by the fast mixing of reactants, explained the effect of the gelling status of carrageenan on properties of precipitate [12].

The objective of this work is to elaborate the protocols for production of a significant amount of $CaCO_3$/hydrogel composites and to demonstrate the possibilities to control the physical properties of mineral particles, with emphasis on their size, surface texture, porosity and shape. Since the biocompatible and degradable polysaccharides (sodium alginate and xanthan gum) and bioactive calcium carbonate polymorphs are used, the composites may be suitable for application in a field of hard tissue engineering or drug delivery. In addition, the obtained results may be used as alternative experimental strategies for preparation of porous and/or monodispersed $CaCO_3$ polymorphs, suitable for use as templates for the preparation of polyelectrolyte multilayer capsules.

2. Results and Discussion

The precipitation in gelling environment has been initiated by the fast mixing of reactants in order to enable a rapid formation of gel and apparently instantaneous establishment of supersaturation [12]. Both polysaccharides, xanthan and alginate, are anionic polyelectrolytes with similar chemical functionalities attached to molecules' backbone (carboxylate, hydroxide). Indeed, alginate contains about one COOH, while xanthan less than 0.4 COOH per sugar unit. The alginate hydrogels are formed by crosslinking their molecules with divalent cations, while the formation of xanthan gel is caused by releasing the water molecules that are attached to polysaccharide molecules and hydrogen bonding of chains [38–42]. The pore size distribution of both gels was controlled by varying the polysaccharide molecule concentration.

The results of morphological and structural analyses of $CaCO_3$ precipitated in gels were compared to referent bulk-precipitation systems. In this way the effects caused by the space confinement and charge density may be discerned from otherwise dominating factors for precipitation of slightly soluble salts, like supersaturation and hydrodynamics. Thus, the initial supersaturation was be set to be relatively high, in order to undoubtedly exceed the threshold values for onset of nucleation in both systems. In all systems the concentrations of precipitating components were identical: $c(CaCl_2) = c(Na_2CO_3) = 0.066$ mol dm^{-3}, which correspond to supersaturations expressed with respect to amorphous calcium carbonate (ACC), $S_C = 89.2$ and $S_{ACC} = 8.1$, respectively. Indeed, the addition of polysaccharides affects the concentration of unbound calcium ions and the activity of all reactants present in the system, so it is rather difficult to calculate the actual supersaturation in gelling systems. Therefore, the applied concentrations of reactants were relatively high in order to ensure that the threshold value for the onset of nucleation was exceeded in both systems and at all concentrations of hydrogels. Indeed, fast and intensive precipitation was observed in all systems.

Three types of precipitation experiments in gel were performed in order to discriminate possible hydrodynamic effects (order of addition of reactants), or the adjustment of pH, which may influence the distribution of charges of polysaccharide molecules. Thus, in the system Ca-gel, pH = 10.5, Na_2CO_3 solution was introduced into the $CaCl_2$/polysaccharide solution with respective concentration of alginate or xanthan. The pH of $CaCl_2$ was pre-adjusted to 10.5. The system Ca-gel, pH = 9.0, is identical, but the pH of the $CaCl_2$ was pre-adjusted to 9.0. The order of addition of reactants was changed in the CO_3-gel, pH = 10.5 system, in which the $CaCl_2$ solution (pH = 10.5) was rapidly introduced into the Na_2CO_3/polysaccharide solutions of the appropriate concentration of polysaccharide.

However, in the respective model systems (identical concentrations of reactants, but without presence of polysaccharide), a mixture of amorphous calcium carbonate (ACC), calcite and vaterite precipitated immediately after mixing the reactants. Transformation of unstable phases into the calcite was completed after about 24 h. Figure S10 shows typical calcite crystals isolated from the system. Similar precipitation/transformation pattern, according to which only calcite remained in the system after 24 h, was also observed in the systems of higher and lower supersaturation ($c(CaCl_2) = c(Na_2CO_3) = 0.1$ mol dm^{-3} and $c(CaCl_2) = c(Na_2CO_3) = 0.033$ mol dm^{-3}).

2.1. $CaCO_3$ Precipitation in Xanthan Gels

The concentrations of xanthan used for precipitation experiments varied in the range from 0.20–2.00 wt % with respect to water and, in all systems, the formation of precipitate occurred immediately after the addition of calcium or carbonate solution. The results of structural analyses (P-XRD) and morphological observations (SEM) of precipitates are reported in Table 1 and in Figure S1a. Typical X-ray diffractograms and respective FT-IR spectra are also shown (Figures S2, S3 and S6). Hence, it is shown that at lower gel concentrations, c_{xan} = 0.20 wt % and 0.35 wt %, the precipitate obtained five days after initiating the process, consists predominantly of calcite, with traces of vaterite. At a moderate concentration of gel, c_{xan} = 0.40 wt %, calcite is still the predominant phase unless in the system Ca-gel, pH = 10.5, about 39 wt % of vaterite is mixed with calcite. At the highest gel concentration, c_{xan} = 2.00 wt %, vaterite was found to be significantly present in all systems.

Table 1. Mineralogical composition, shape and average size (referred to the longest axis of single particle or aggregate) of precipitate (calcite and vaterite) prepared in different xanthan gels and $c_i(CaCl_2) = c_i(Na_2CO_3)$ = 0.066 mol dm^{-3}, t = 5 days.

	c_{xan}/wt %	w_{calc}/wt %	Shape	L/μm [#]
Ca-gel pH = 9.0	0.20	99	*c*-axis elongated rhombohedra	15(5)
	0.35	95	*c*-axis elongated rhombohedra	10(5)
	0.40	99	etched rhombohedra	10(5)
	2.00	21	etched rhombohedra-spheres	10(5)–10(5)
Ca-gel pH = 10.5	0.20	100	Rhombohedra	10(5)
	0.35	99	Rhombohedra	10(5)
	0.40	61	etched rhombohedra-spheres	10(5)–10(5)
	2.00	19	etched rhombohedra-spheres	10(5)–10(5)
CO_3-gel pH = 10.5	0.20	100	rhombohedra *	15(5)
	0.35	100	rhombohedra *	10(5)
	0.40	100	rhombohedra *	10(5)
	2.00	54	Rhombohedra-spheres	10(5)–10(5)

* Indicates the presence of a high number of hemispherical cavities on the {10.4} faces. [#] Values in parenthesis indicates the standard deviation.

The results of morphological analyses (SEM) are consistent with structural analyses of precipitate. Thus, Figure 1 shows the typical morphologies of crystals isolated five days after initiating the precipitation in different xanthan gels. In the system Ca-gel, pH = 9.0, and lower concentrations of xanthan (c_{xan} = 0.20 wt % and 0.35 wt %) the obtained calcite single crystals were elongated along the *c* axis: Some of the latter showed hemispherical cavities. In the precipitate obtained by using, c_{xan} = 0.40 wt %, the calcite crystals are actually the assembly of subcrystals, etched on the {104} faces. At c_{xan} = 2.00 wt % the SEM showed predominantly single spheres having a smooth surface and few elongated calcite crystals showing {011} faces and {104} faces. In the Ca-gel, pH = 10.5 system and c_{xan} = 0.20 wt %, calcite appeared as {104} rhombohedra single crystals in which some {104} showed hemispherical cavities. At a c_{xan} = 0.35 wt % the calcite crystals showed aggregation and the morphology was not regular, while at increased concentration, c_{xan} = 0.40 wt %, the rhombohedral calcite crystals were elongated along the *c*-axis. At the highest concentration, c_{xan} = 2.00 wt %, the precipitate consists of spheres, having a smooth surface and sometimes joined with calcite crystal with cavities. In some cases, the spheres fill calcite crystals (Figure S8). The precipitates observed in the CO_3-gel pH = 10.5 systems, c_{xan} < 2.0 wt %, were rather similar to Ca-gel, pH = 10.5 and c_{xan} = 0.35 wt %: Calcite appeared in a form of single crystals in which some of the {104} faces showed cavities. However, when the applied xanthan concentration was the highest, c_{xan} = 2.00 wt %, the precipitate consisted of {104} rhombohedral calcite and aggregates of spheres with rough surfaces.

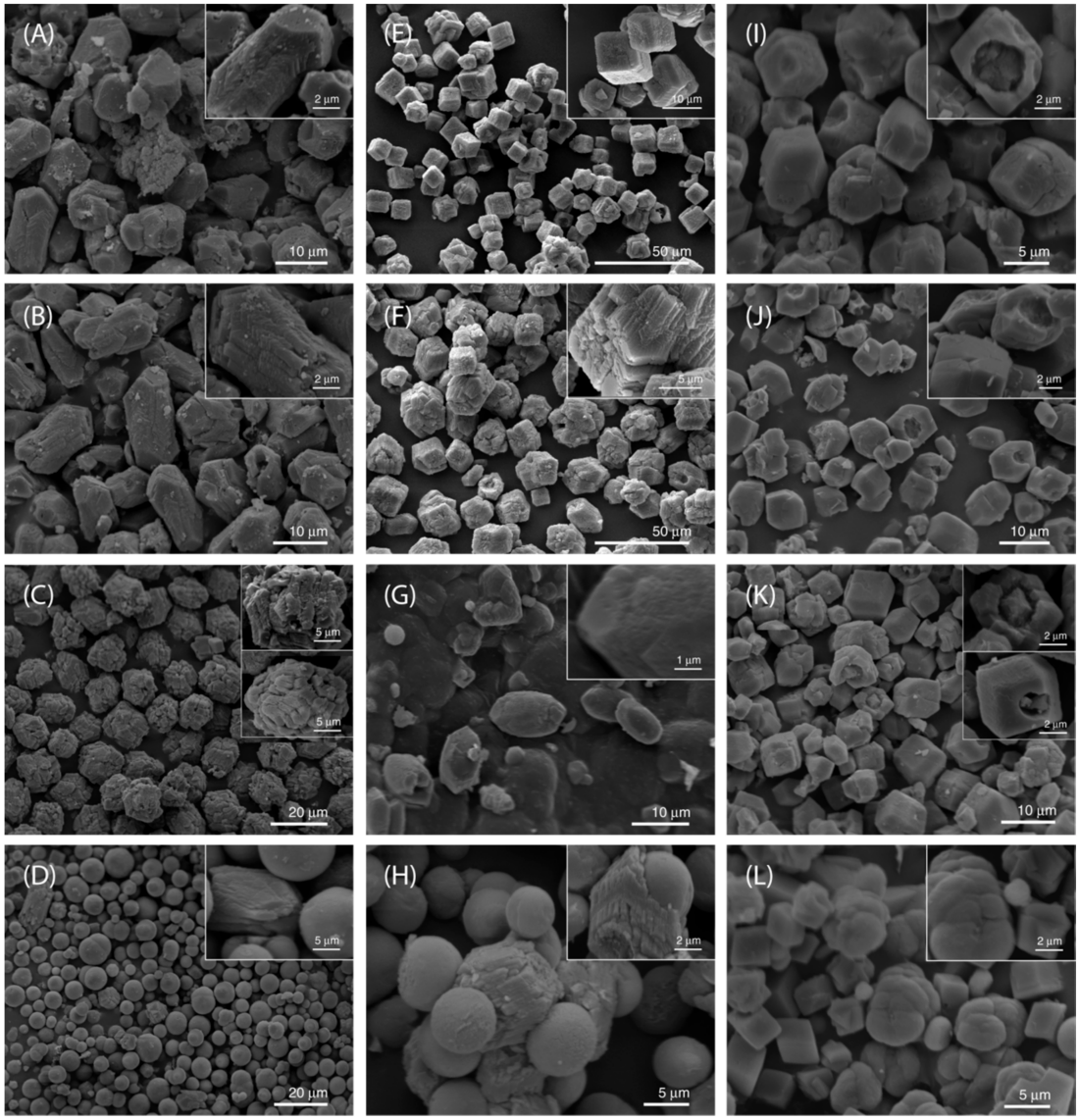

Figure 1. SEM micrographs of $CaCO_3$ precipitated in xanthan hydrogels, prepared by different procedures and concentration of polysaccharide. Precipitate was isolated 5 days after initiating the process. (**A**–**D**) sample prepared using the system Ca-gel, pH = 9.0 and c_{xan} = 0.20 wt % (**A**); c_{xan} = 0.35 wt % (**B**); c_{xan} = 0.40 wt % (**C**); c_{xan} = 2.00 wt % (**D**). (**E**–**H**) sample prepared using the system Ca-gel, pH = 10.5 and c_{xan} = 0.20 wt % (**E**); c_{xan} = 0.35% (**F**); c_{xan} = 0.40 wt % (**G**); c_{xan} = 2.00 wt % (H). (**I**–**L**) sample prepared using the system CO_3-gel, pH = 10.5 and c_{xan} = 0.20 wt % (**I**); c_{xan} = 0.35% (**J**); c_{xan} = 0.40 wt % (**K**); c_{xan} = 2.0 wt % (**L**). The images are representative of the entire populations of particles.

Similar gradual change of calcite morphology with increasing xanthan gel concentration (from compact rhombohedral crystals to spherical aggregates) has been described in the system in which crystallization was initiated in $(NH_4)_2CO_3$-$CaCl_2$ systems [43]. The authors used xanthan as a model of the exopolysaccharides excreted by soil bacteria, which are supposed to be responsible for accumulation of terrestrial carbonates. The observed formation of spherical calcite and vaterite was explained with increased diffusivity (viscosity) of the medium and the presence of carboxyl groups, which were additionally introduced into a form of acidic amino acids.

It should be emphasized that in all xanthan systems and c_{xan} = 2.00 wt %, a mixture of calcite and vaterite precipitated. Thus, spherical aggregates of vaterite, calcite rhombohedra or rhombohedral

calcite aggregates were observed. High fraction of not-transformed vaterite in these systems can be explained by assuming a simultaneous nucleation and crystal growth of metastable and stable polymorphs and subsequent transformation of metastable phases, either by solution mediated, or a solid-state mechanism. During the transformation process, dissolution of vaterite and growth of calcite crystals occur simultaneously. It was found previously that in pure aqueous systems [44] vaterite dissolution is controlled by the diffusion of constituent ions (Ca^{2+} and CO_3^{2-}) away from the crystal surfaces, while calcite growth is controlled by surface process. At conditions of high concentration of macromolecules and restricted diffusivity, vaterite dissolution becomes the rate determining step of the overall transformation process. Therefore, at the highest xanthan concentrations, the vaterite content is still high. In most of the systems, size of the particles varied in the range from 10 to 15 μm, without any systematic correlation between their sizes and xanthan concentration. In addition, in the systems of the highest gel concentration (c_{xan} = 2.0 wt %) two polymorphs could be observed: Spherical vaterite particles and prismatic calcite, which are of different size. However, the vaterite aggregates, which are trapped within a calcite crystal, indicate the initial growth of both polymorphs in a limited space (Figure S8).

In order to prove the incorporation of xanthan molecules by $CaCO_3$, the thermogravimetric analyses (TGA) of selected samples have been done. Thus, in the system Ca-gel, pH = 10.5, c_{xan} = 0.2 wt %, a mass loss of about 0.8%, in the range of temperatures between 50–150 °C was observed. This loss corresponds to water molecules, while loss of about 1.0%, obtained within the range, 150–400 °C, corresponds to the decomposition of the organic matter. In the similar system, Ca-gel, pH = 10.5, c_{xan} = 0.35 wt %, about 0.3% of water (60–150 °C) and 0.9% of organic matter (150–400 °C) detected. The results are comparable to those described in literature for calcite precipitation in the presence of relatively low content of xanthan (c = 0.05%) and different initial concentrations of Ca^{2+} and CO_3^{2-} [45]. Thus, the authors found that about 1% of xanthan could be incorporated into the calcite which grow in system [Ca^{2+}] = [CO_3^{2-}] = 16 mmol dm^{-3}, while at higher concentration, [Ca^{2+}] = [CO_3^{2-}] = 32 mmol dm^{-3}, the incorporated amount is lower, 0.27%. Similar investigations in the agarose hydrogels of different strengths and degree of entanglements [7,46] showed exactly the opposite trend of incorporation of gelling polysaccharide into the calcite structure. Thus, the increase of the Ca^{2+} concentration from 5 mmol dm^{-3} to 30 mmol dm^{-3} caused the increase of the agarose incorporation in the range from about 0.5 wt % to 0.9 wt %. The authors also proposed different models of incorporation, which assumed a competition between parameters like the strength of the gel, growth rate or specific crystal/agarose interactions.

2.2. $CaCO_3$ Precipitation in Alginate Gels

The concentrations of alginate used for precipitation experiments varied in the range from 0.20 wt % to 2.00 wt % with the respect to water and precipitation started immediately after mixing the reactants. The results of structural analyses of precipitate (P-XRD and FT-IR) are shown in Table 2 and in Figure S1, while Figures S4, S5 and S7 show the typical X-ray diffractograms and FT-IR spectra. Thus, in the Ca-gel, pH = 10.5, mixture of calcite and vaterite was observed, while predominantly calcite precipitated in the Ca-gel, pH = 9.0 and CO_3-gel, pH = 10.5 systems. In the Ca-gel, pH = 9.0 and lowest alginate concentration, vaterite was observed as well. In all gelling systems, the largest $CaCO_3$ particles were observed at the lowest alginate concentration (c_{alg} = 0.20 wt %). However, at higher gel concentrations, the average size of the particles decreased but no distinct correlation between the size distribution and gel concentration was observed.

Table 2. Mineralogical composition, shape and average size (referred to the longest axis of single particle or aggregate) of precipitate (calcite and vaterite) prepared in different alginate gels and $c_i(CaCl_2) = c_i(Na_2CO_3) = 0.066$ mol dm^{-3}, $t = 5$ days.

	c_{alg}/wt %	w_{calc}/wt %	Shape	L/μm #
Ca-gel pH = 9.0	0.20	78	rhombohedra */spheres	10(3)–5(1)
	0.50	100	rhombohedra	5(2)
	0.80	100	rhombohedra *	5(2)
	2.00	100	rhombohedra *	5(2)
Ca-gel pH = 10.5	0.20	63	rhombohedra *-spheres	15(5)–5(2)
	0.50	76	rhombohedra *-spheres	10(5)–5(3)
	0.80	61	rhombohedra *-spheres	10(5)–5(4)
	2.00	77	rhombohedra *-spheres	10(5)–5(3)
CO_3-gel pH = 10.5	0.20	100	rhombohedra *	15(5)
	0.50	100	rhombohedra	10(3)
	0.80	100	rhombohedra	10(5)
	2.00	100	rhombohedra	10(5)

* Indicates the presence of a high number of hemispherical cavities on the {10.4} faces. # Values in parenthesis indicates the standard deviation.

Typical SEM micrographs of the dried $CaCO_3$ samples, precipitated in different alginate gels are shown in Figure 2. Thus, calcite crystals precipitated in the CO_3-gel, pH = 10.5 appeared in the form of stack-like or polyhedral aggregates, built up of prismatic primary particles. On the other hand, the rosette-like aggregates are predominant calcite forms in both Ca-gels. This is in agreement with findings of some other authors that precipitated $CaCO_3$ in presence of alginate or xanthan, but at concentrations lower than critical for gel formation [45,47]. The predominant formation of rosette-like calcite was explained by its nucleation on a gelled microparticles template. However, predominant growth of stuck-like calcite morphology in the xanthan systems has been explained by its nucleation directly on ionized carboxylate groups along the backbone of polysaccharide molecules (see SI: Description of molecular gelling process) [38–42]. In comparison to literature data, the systems investigated in this work are additionally complicated by strong gel formation and initial precipitation of metastable and stable solid phases in close physical contact. Thus, Figure S9, shows vaterite and calcite particles merged in a single phase in the alginate system in which vaterite to calcite transformation was not completed (Ca-gel, pH = 10.5, c(alg) = 0.8 wt %). Contrarily, in the systems in which the solution-mediated process of transformation was completed, the cavities in the calcite crystals are visible (CO_3-gel, pH = 10.5, c_{alg} = 0.8 wt % and Ca-gel, pH = 9.0, c_{alg} = 0.8 wt %). The effect is stronger than in the xanthan gels of comparable concentration, which can be explained by difference between their gelling mechanism: Strong crosslinking between alginate molecules with divalent cations, versus the hydrogen bonding in xanthan. In addition, it should be considered that xanthan contains less COOH groups that could initially interact with solid phases (1 COOH per monosaccharide unit in alginate, versus 2/5 COOH per monosaccharide in xanthan).

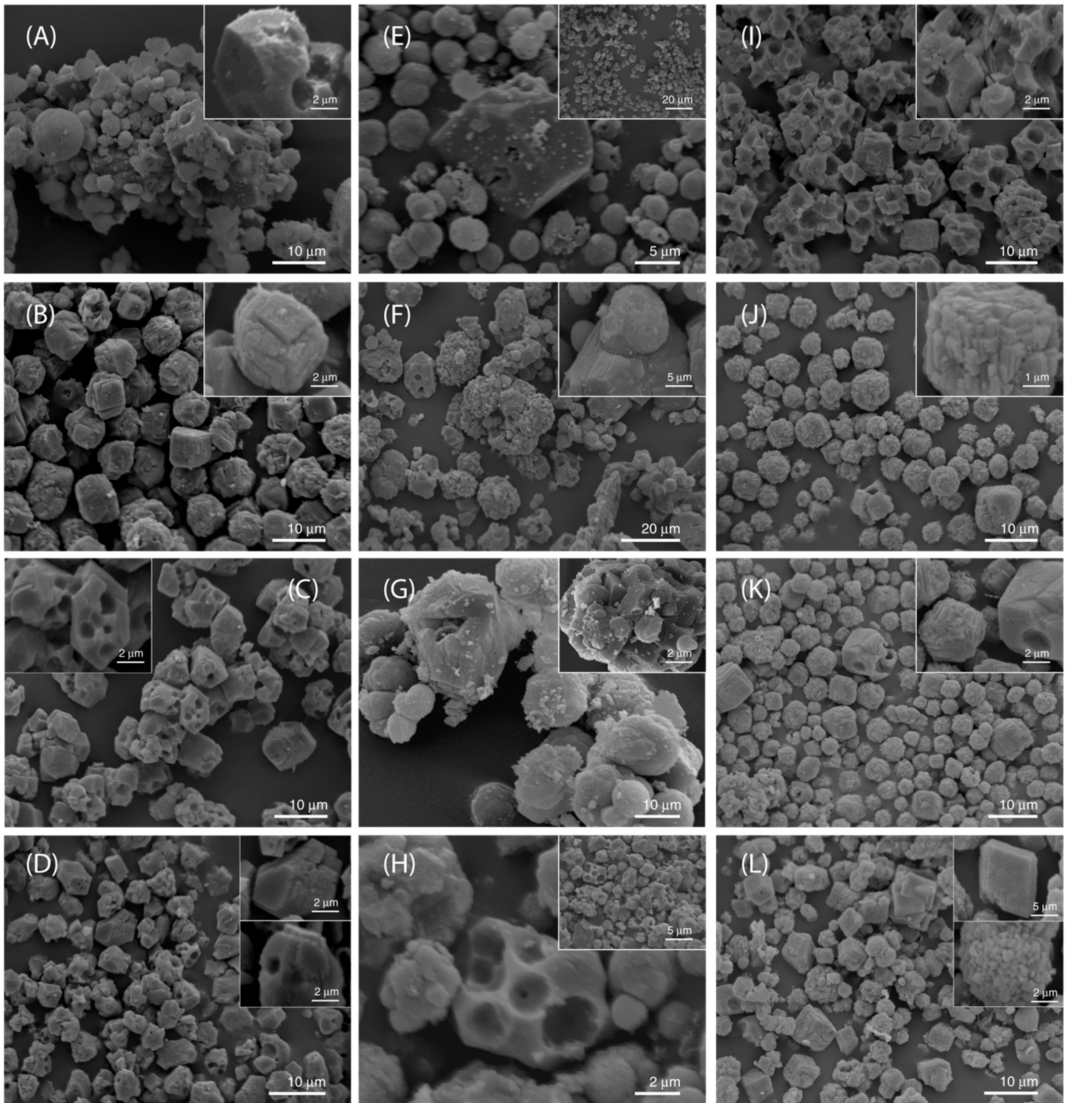

Figure 2. SEM micrographs of $CaCO_3$ precipitated in alginate hydrogels, prepared by different procedures and concentration of polysaccharide. Precipitates are isolated 5 days after initiating the process. (**A**–**D**) sample prepared using the system Ca-gel, pH = 9.0 and c_{alg} = 0.2 wt % (**A**); c_{alg} = 0.5 wt % (**B**); c_{alg} = 0.8 wt % (**C**); c_{alg} = 2.0 wt % (**D**). (**E**–**H**) sample prepared using the system Ca-gel, pH = 10.5 and c_{alg} = 0.2 wt % (**E**); c_{alg} = 0.5 wt % (**F**); c_{alg} = 0.8 wt % (**G**); c_{alg} = 2.0 wt % (**H**). (**I**–**L**) sample prepared using the system CO_3-gel, pH = 10.5 and c_{alg} = 0.2 wt % (**I**); c_{alg} = 0.5 wt % (**J**); c_{alg} = 0.8 wt % (**K**); c_{alg} = 2.0 wt % (**L**). The images are representative of the entire populations of particles.

2.3. Kinetics of $CaCO_3$ Phase Transition in the Alginate Gels

The assumed initial and simultaneous formation of several $CaCO_3$ phases in alginate gels was confirmed by time resolved precipitation experiments in a moderately strong gelling environment (Ca-gel, pH = 9.0, c_{alg} = 0.8 wt %). Figure 3A shows SEM micrographs of mineral particles isolated immediately after formation of precipitate and after termination of the process (Figure 3B). Indeed, typical vaterite spherulitic aggregates can be seen at the early stages of the process, while irregular prismatic calcite crystals with spherical imprints were found at later stages. The existence of both, metastable and stable polymorphs in alginate gelling systems are similar to findings of Dias-Dosque et al. [48], obtained by spin-coating techniques and a slow CO_2 diffusion. The semi quantitative FT-IR analysis of mineral samples [49] separated from the gel at time intervals coincide with the SEM observations (Figure 4). It is shown that vaterite content decreased from about 80 wt % at

the beginning of the process and dropped to zero after 24 h. The observed relatively fast transformation of vaterite crystals is apparently in contradiction to the results of $CaCO_3$ growth in the system in which alginate and Ca^{2+} have slowly released from respective gels [29]. In these systems, in which CO_2 diffusion technique was used, vaterite remained stabilized for 8 days, which is probably the consequence of continuous supply of Ca^{2+} and CO_3^{2-}. Their concentrations were obviously high enough to keep the supersaturation level above the vaterite solubility and, as a result, hindered the dissolution. Unfortunately, such experimental setup does not provide the information on solution composition, which is crucial for understanding the mechanisms of formation of specific phases. However, in the experimental setup applied in this work, the initial supersaturation could be estimated and the continuous sampling for the FT-IR analyses applied. The analyses indicated that, besides the crystalline polymorphs, the amorphous $CaCO_3$ also existed at the early stages of the process. It was identified according to the normal vibration frequencies of carbonate ions at about 1490 and 1430 cm^{-1} (ν_{3a}, ν_{3b}), 1080 cm^{-1} (ν_1), 866 cm^{-1} (ν_2), 725 and 690 cm^{-1} (ν_{4a}, ν_{4b}) [50–52]. Since, ν_2 and ν_4 bands cannot be detected in the mixtures with high content of polymorphs, the ratios of the intensities of ν_2 and ν_4 absorption bands of calcite were measured [53,54]. In the case of pure calcite, the ratio is about 3, while in the mixtures with ACC, it increases as a consequence of the absence of ν_4 absorption of ACC in the 713 cm^{-1} region. Thus, it was found that the ν_2/ν_4 of the sample isolated at the beginning of the crystallization was about 7.7, while after 24 h it drops to 2.3.

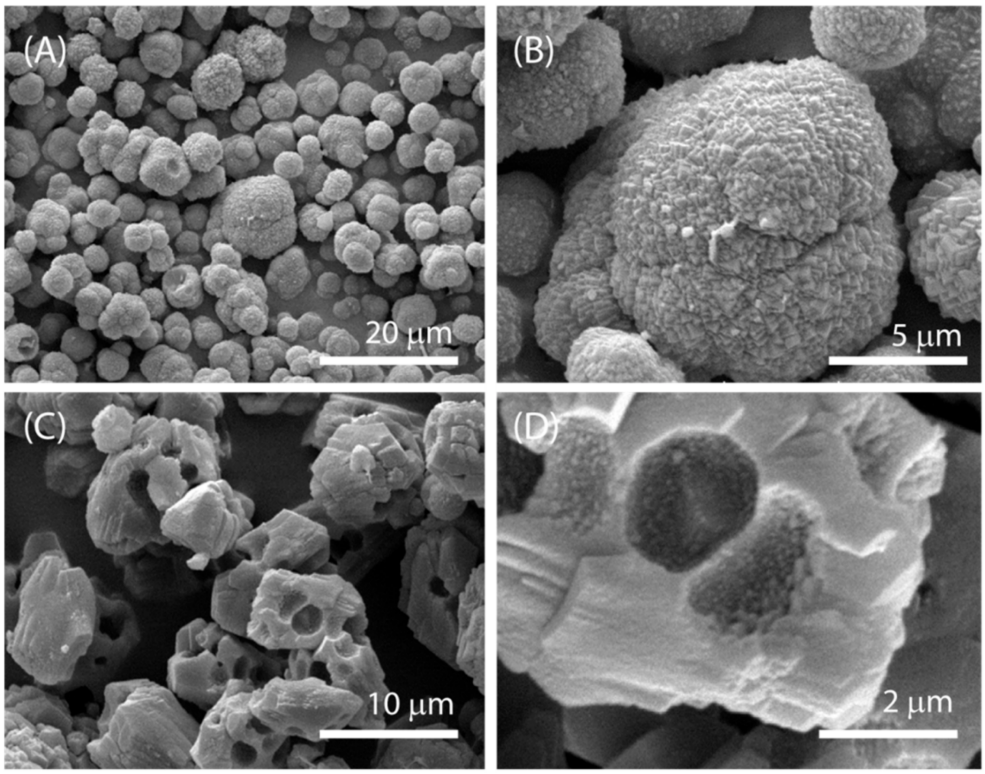

Figure 3. SEM micrographs of $CaCO_3$ precipitated in Ca-gel, pH = 9.0 and c_{alg} = 0.8 wt %, isolated from the system immediately after onset of the crystallization (**A**,**B**) and after 24 h (**C**,**D**). The higher magnification micrographs are shown on the right side. The images are representative of the entire populations of particles.

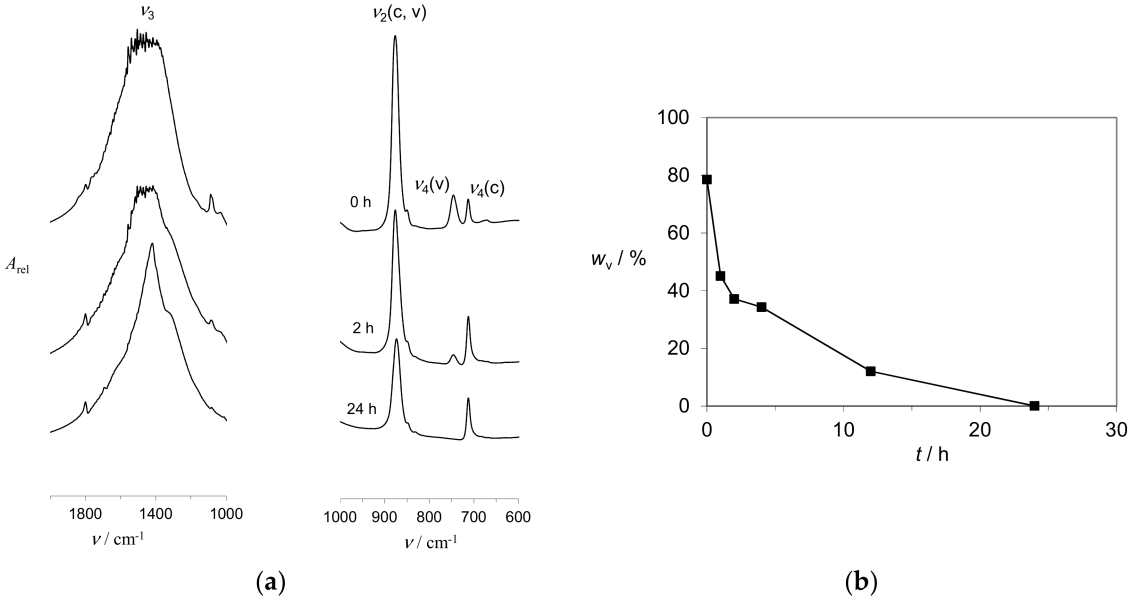

Figure 4. (**a**) The FT-IR spectra of typical $CaCO_3$ samples precipitate in Ca-gel (pH = 9.0; c_{alg} = 0.8 wt %) and separated at respective time intervals. The absorption bands of calcite and vaterite at 712 cm^{-1} and 745 cm^{-1} are indicated. (**b**) The change of vaterite/calcite content with time, estimated by comparison of the intensities of ν_4 normal vibrations of carbonate ions in vaterite (v) and calcite (c).

The expected incorporation of the alginate molecules into the $CaCO_3$ precipitate was tested by TGA analyses of the samples isolated at selected time intervals. The results show (Table S1) that the precipitate which consisted of calcite (t = 24 h) incorporated significantly less organic matter and water in comparison to systems containing vaterite. However, no straightforward correlation between the TG data and the vaterite or calcite content was found, which indicates that the water and organic matter are not uniformly distributed within the gel and mineral phases. However, the correlation can be found between the vaterite content and the total amount of incorporated water and alginate macromolecules. Similar measurements were made in the system Ca-gel, pH = 10.5, c_{alg} = 0.8 wt %, in which about 39% of vaterite was found after five days of aging. It was determined that about 3.2% of water and 5.3% of organic matter are incorporated into the precipitate, which is qualitatively consistent with data obtained from kinetics.

3. Materials and Methods

The chemicals used to prepare reactant solutions, $CaCl_2$ and Na_2CO_3, were analytically pure and the deionized water was of high quality (conductivity < 0.055 μS cm^{-1}). Sodium carbonate solution, c = 0.20 mol dm^{-3}, was prepared by dissolving anhydrous Na_2CO_3 in water, while calcium chloride solution, c = 0.20 mol dm^{-3}, was made by diluting appropriate $CaCl_2$ stock.

The polysaccharides used for gel preparation were kindly supplied by Danicso. Xanthan gum was produced by a fermentation process of bacteria *Xanthomonas campestris*, while sodium alginate was produced from brown seaweed, mainly *Laminaria digitata* species. The appropriate polysaccharide stock solutions were prepared by the addition of respective amount of dry powder into deionized water at 70–80 °C and intensive stirring until complete dissolution. Three different protocols of simultaneous calcium carbonate precipitation and gel formation were employed.

3.1. CO_3-Gel, pH = 10.5

50 cm^3 of hot (70–80 °C) polysaccharide (alginate or xanthan) solution of respective concentration was mixed with 50 cm^3 of Na_2CO_3 solution (c = 0.20 mol dm^{-3}, pH = 11.5) and intensively stirred. Precipitation was initiated by rapid addition of 50 cm^3 of $CaCl_2$ solution (c = 0.20 mol dm^{-3}) into

100 cm^3 of thus prepared Na_2CO_3/polysaccharide mixture. The pH of $CaCl_2$ solution was previously adjusted by the addition of NaOH, to the value, pH = 10.5. The obtained suspension was aged for 5 days at room temperature.

3.2. C-Gel, pH = 9.0

50 cm^3 of hot (70–80 °C) polysaccharide (alginate or xanthan) solution of respective concentration was mixed with 50 cm^3 of $CaCl_2$ solution (c = 0.20 mol dm^{-3}) and intensively stirred. The pH of $CaCl_2$ solution was previously adjusted by the addition of NaOH to the value, pH = 9.0. Precipitation was initiated by rapid addition of 50 cm^3 of Na_2CO_3 solution (c = 0.20 mol dm^{-3}, pH = 11.5) into 100 cm^3 of thus prepared $CaCl_2$/polysaccharide mixture. The obtained suspension was aged for 5 days at room temperature.

3.3. Ca-Gel, pH = 10.5

50 cm^3 of hot (70–80 °C) polysaccharide (alginate or xanthan) solution of respective concentration was mixed with 50 cm^3 of $CaCl_2$ solution (c = 0.20 mol dm^{-3}) and intensively stirred. The pH of $CaCl_2$ solution was previously adjusted by the addition of NaOH to the value, pH = 10.5. Precipitation was initiated by rapid addition of 50 cm^3 of Na_2CO_3 solution (c = 0.20 mol dm^{-3}, pH = 11.5) into 100 cm^3 of thus prepared $CaCl_2$/polysaccharide mixture. The obtained suspension was aged for 5 days at room temperature.

3.4. Model System

Precipitation was initiated by rapid addition of 50 cm^3 of Na_2CO_3 solution (c = 0.20 mol dm^{-3}, pH = 11.5) into 100 cm^3 of magnetically stirred $CaCl_2$ solution, (c = 0.20 mol dm^{-3}, pH = 6.7). The progress of the reaction was followed by measuring the pH. The system was aged for 24 h.

At the end of each experiment, the suspension was centrifuged, the precipitate was washed several times with saturated calcite solution and dried at 105 °C for 3 h. Thermogravimetric analyses of precipitates were performed by means of Mettler TG 50 thermobalance, equipped with TC 10 TA processor, at rate 10 K/min. Qualitative and semi quantitative composition of the dried precipitate was determined by means of FT-IR spectroscopy (FT-IR Bruker, Tensor II) using KBr pellet technique [35] and by X-ray powder diffraction (XRD) using an automatic Philips diffractometer, model PW1820 (CuKα radiation, graphite monochromator, proportional counter) in Bragg-Brentano geometry. The diffraction intensities were measured in the angular range $10° \leq 2\Theta \leq 70°$. Step size was set to 0.02° of 2θ with measuring time of 2 s per step. Calcite and vaterite were identified according to the ICDD Powder Diffraction File [55]. In order to determine the mole fractions of calcite and vaterite in the samples, a calibration curve, correlating the intensity ratios of selected diffraction lines and the mole ratio of calcite and vaterite, was constructed. The morphologies of the precipitate were observed by optical microscopy (Orthoplan photographic microscope, E. Leitz, Wetzlar, Germany) and by scanning electron microscopy, SEM (Hitachi 6400) operating at 20 kV. For the SEM observations, the samples were glued by a carbon tape on the aluminum stub and gold sputtered.

Calculation of the initial solution composition (supersaturation) was based on the known total calcium chloride and sodium carbonate concentrations and the known NaOH concentration used for pH adjustment. The initial supersaturation was defined as relative supersaturation, $S = (\Pi/K_{sp})^{1/2}$, where Π is the ion activity product, $\Pi = a(Ca^{2+})\cdot a(CO_3^{2-})$, and K_{sp} is the thermodynamic solubility product of calcite ($K_{sp} = 3.313 \times 10^{-9}$), vaterite ($K_{sp} = 1.221 \times 10^{-8}$) or amorphous calcium carbonate (ACC) ($K_{sp} = 3.976 \times 10^{-7}$) [37] at 25 °C. Detailed calculation procedure, which considers the respective protolytic equilibria and equilibrium constants, as well as the charge and mass balance equations, was shown previously [56,57]. However, it should be emphasized that in the case of precipitation in gels, the presence of the respective polysaccharide was not considered so the calculated initial supersaturation is given only for comparison with bulk precipitation experiments.

4. Conclusions

Precipitation of calcium carbonate was investigated in xanthan and alginate hydrogels in which the concentration of polysaccharide molecules varied in the range from 0.2 to 2.0%.

Precipitation was performed simultaneously with the gel formation and was initiated by a fast addition of reactants (Ca^{2+} or CO_3^{2-} solutions) into hot CO_3-polysaccharid or Ca-polysaccharide solutions, respectively. Relatively high initial supersaturation was selected in order to exceed the threshold values for starting the nucleation in both gelling systems and at all concentrations of macromolecules. In addition, high initial supersaturation provided the environment for initial and simultaneous formation of different polymorphic modification of calcium carbonate. Simultaneous nucleation and growth of spherical vaterite aggregates and prismatic calcite crystals in the confined space resulted in the formation of hybrid, ingrown structures. After dissolution of vaterite, which is a result of aging of the precipitate, calcite crystals with spherical imprints remained.

In the model systems (no polysaccharide), a mixture of calcite, vaterite and amorphous calcium carbonate precipitated initially, but due to the solution-mediated process of transformation, only calcite remained in the solution after 24 h. Transformation (dissolution) of ACC typically finished after five min.

In the presence of lowest concentrations of xanthan gel, the precipitate aged for five days consisted predominantly of calcite single crystals with developed {011} faces, elongated along *c* axis and capped with {104} faces. At moderate xanthan concentrations, the porous polyhedral aggregates were found after five days of aging. At the highest xanthan gel concentration, a substantial amount of not-transformed vaterite was observed in all systems, thus pointing out to the strong inhibition of vaterite dissolution.

In the CO_3-alginate gels of all concentrations, calcite was the only calcium carbonate polymorph found after five days of aging, while in the Ca-gels the vaterite was found as well. In the CO_3-gels, calcite appeared in a form of microcrystalline aggregates, while in Ca-gels the rosette-like or stuck-like monocrystals was found.

Time resolved crystallization experiments in moderately strong Ca-alginate hydrogels, showed that a mixture of calcite, vaterite and amorphous calcium carbonate formed initially. After 24 h of aging, only calcite remained in suspension. In comparison to the model system, transformation of amorphous calcium carbonate was significantly inhibited and it was detected even after four h of aging.

Calcite samples isolated from gelling systems typically incorporate less than 1% of water molecules and about 1% of macromolecules. The incorporation of water into the samples containing vaterite is significantly higher and up to 6.8% was determined. The content of absorbed macromolecules is also much higher and more than 3% was found in all systems.

Described one-step protocols may be useful for preparation of biocompatible $CaCO_3$/alginate or $CaCO_3$/xanthan hydrogel composites, with different gel strength, mineral phase composition and adjustable micro or macro porosity. Indeed, such mixtures may be suitable for diverse applications in the hard tissue engineering and/or drug delivery.

Supplementary Materials: The following are available online at www.mdpi.com/2073-4352/7/12/355/s1.

Acknowledgments: This work was supported (Damir Kralj and Cleo Kosanović) by the Croatian Science Foundation under the project (IP-2013-11-5055). Giuseppe Falini and Simona Fermani thank the Consorzio Interuniversitario per la Chimica dei Metalli nei Sistemi Biologici for the support.

Author Contributions: The manuscript was written through contributions of all authors. All authors have given approval to the final version of the manuscript.

Conflicts of Interest: The authors declare no conflict of interest.

References

1. Brecevic, L.; Kralj, D. On calcium carbonates: From fundamental research to application. *Croat. Chem. Acta* **2007**, *80*, 467–484.

2. Sommerdijk, N.A.J.M.; de With, G. Biomimetic $CaCO_3$ mineralization using designer molecules and interfaces. *Chem. Rev.* **2008**, *108*, 4499–4550. [CrossRef] [PubMed]
3. Gebauer, D.; Völkel, A.; Cölfen, H. Stable prenucleation calcium carbonate clusters. *Science* **2008**, *322*, 1819–1822. [CrossRef] [PubMed]
4. Meldrum, F.C.; Cölfen, H. Controlling mineral morphologies and structures in biological and synthetic systems. *Chem. Rev.* **2008**, *108*, 4332–4432. [CrossRef] [PubMed]
5. Demichelis, R.; Raiteri, P.; Gale, J.D. Structure of hydrated calcium carbonates: A first-principles study. *J. Cryst. Growth* **2014**, *401*, 33–37. [CrossRef]
6. Carlson, W.D. The polymorphs of $CaCO_3$ and the aragonite-calcite transformation. *Rev. Mineral. Geochem.* **1983**, *11*, 191–225.
7. Asenath-Smith, E.; Li, H.; Keene, E.C.; Seh, Z.V.; Estroff, L.A. Crystal growth of calcium carbonate in hydrogels as a model of biomineralization. *Adv. Funct. Mater.* **2012**, *22*, 2891–2914. [CrossRef]
8. Flory, P.J. Introductory lecture. *Faraday Discuss. Chem. Soc.* **1974**, *57*, 7–18. [CrossRef]
9. Estroff, L.A.; Hamilton, A.D. Water gelation by small organic molecules. *Chem. Rev.* **2004**, *104*, 1201–1218. [CrossRef] [PubMed]
10. Nindiyasari, F.; Fernández-Díaz, L.; Griesshaber, E.; Astilleros, J.M.; Sánchez-Pastor, N.; Schmahl, W.W. Influence of gelatin hydrogel porosity on the crystallization of $CaCO_3$. *Cryst. Growth Des.* **2014**, *14*, 1531–1542. [CrossRef]
11. Max, A.; Lauffer, M.A. Theory of diffusion in gels. *Biophys. J.* **1961**, *1*, 205–213.
12. Kosanovic, C.; Falini, G.; Kralj, D. Mineralization of calcium carbonates in gelling media. *Cryst. Growth Des.* **2011**, *11*, 269–277. [CrossRef]
13. Xie, M.; Olderoy, M.O.; Andreassen, J.P.; Selbach, S.M.; Strand, B.L.; Sikorski, P. Alginate-controlled formation of nanoscale calcium carbonate and hydroxyapatite mineral phase within hydrogel networks. *Acta Biomater.* **2010**, *6*, 3665–3675. [CrossRef] [PubMed]
14. Munro, N.H.; McGrath, K.M. Biomimetic approach to forming chitin/aragonite composites. *Chem. Commun. (Camb.)* **2012**, *48*, 4716–4718. [CrossRef] [PubMed]
15. Volodkin, V.; Petrov, A.I.; Prevot, M.; Sukhorukov, G.B. Matrix polyelectrolyte microcapsules: New system for macromolecule encapsulation. *Langmuir* **2004**, *20*, 3398–3406. [CrossRef] [PubMed]
16. Trushina, D.B.; Bukreeva, T.V.; Kovalchuk, M.V.; Antipina, M.N. $CaCO_3$ vaterite microparticles for biomedical and personal care applications. *Mater. Sci. Eng. C* **2014**, *45*, 644–658. [CrossRef] [PubMed]
17. Volodkin, D.; Klitzing, R.; Möhwald, H. Pure protein microspheres by calcium carbonate templating. *Angew. Chem. Int. Ed.* **2010**, *122*, 9444–9447. [CrossRef]
18. Lengert, E.; Saveleva, M.; Abalymov, A.; Atkin, V.; Wuytens, P.C.; Kamyshinsky, R.; Vasiliev, A.L.; Gorin, D.A.; Sukhorukov, G.B.; Skirtach, A.G.; et al. Silver alginate hydrogel micro- and nanocontainers for theranostics: Synthesis, encapsulation, remote release, and detection. *ACS Appl. Mater. Interfaces* **2017**, *9*, 21949–21958. [CrossRef] [PubMed]
19. Parakhonskiy, B.V.; Yashchenok, A.M.; Konrad, M.; Skirtach, A.G. Colloidal micro- and nano-particles as templates for polyelectrolyte multilayer capsules. *Adv. Colloid Interface Sci.* **2014**, *207*, 253–264. [CrossRef] [PubMed]
20. Yashchenok, A.; Parakhonskiy, B.; Donatan, S.; Kohler, D.; Skirtachad, A.; Mohwald, H. Polyelectrolyte multilayer microcapsules templated on spherical, elliptical and square calcium carbonate particles. *J. Mater. Chem. B* **2013**, *1*, 1223–1228. [CrossRef]
21. Yi, Q.; Sukhorukov, G.B. Externally triggered dual function of complex microcapsules. *ACS Nano* **2013**, *7*, 8693–8705. [CrossRef] [PubMed]
22. Donatan, S.; Yashchenok, A.; Khan, N.; Parakhonskiy, B.; Cocquyt, M.; Pinchasik, B.; Khalenkow, D.; Möhwald, H.; Konrad, M.; Skirtach, M. Loading capacity versus enzyme activity in anisotropic and spherical calcium carbonate microparticles. *ACS Appl. Mater. Interfaces* **2016**, *8*, 14284–14292. [CrossRef] [PubMed]
23. Svenskaya, Y.I.; Fattah, H.; Zakharevich, A.M.; Gorin, D.A.; Sukhorukov, G.B.; Parakhonskiy, B.V. Ultrasonically assisted fabrication of vaterite submicron-sized carriers. *Adv. Powder Technol.* **2016**, *27*, 618–624. [CrossRef]
24. Douglas, T.E.L. *Biomimetic Mineralization of Hydrogels in Biomineralization and Biomaterials, Fundamentals and Applications*; Aparicio, C., Ginebra, M., Eds.; Woodhead Publishing: Cambridge, UK; 2015; pp. 291–313.
25. Gkioni, K.; Leeuwenburgh, S.C.; Douglas, T.E.; Mikos, A.G.; Jansen, J.A. Mineralization of hydrogels for bone regeneration. *Tissue Eng. B* **2010**, *16*, 577–585. [CrossRef] [PubMed]

26. Douglas, T.E.L.; Sobczyk, K.; Łapa, A.; Włodarczyk, K.; Brackman, G.; Vidiasheva, I.; Reczyńska, K.; Pietryga, K.; Schaubroeck, D.; Bliznuk, V.; et al. Ca:Mg:Zn:CO_3 and Ca:Mg:CO_3—tri- and bi-elemental carbonate microparticles for novel injectable self-gelling hydrogel–microparticle composites for tissue regeneration. *Biomed. Mater.* **2017**, *12*, 025015. [CrossRef] [PubMed]
27. Jang, J.; Seol, Y.J.; Kim, H.J.; Kundu, J.; Kim, S.W.; Cho, D.W. Effects of alginate hydrogel cross-linking density on mechanical and biological behaviors for tissue engineering. *J. Mech. Behav. Biomed. Mater.* **2014**, *37*, 69–77. [CrossRef] [PubMed]
28. Kuo, C.K.; Ma, P.X. Maintaining dimensions and mechanical properties of ionically crosslinked alginate hydrogel scaffolds in vitro. *J. Biomed. Mater. Res. A* **2008**, *84*, 899–907. [CrossRef] [PubMed]
29. Corni, I.; Harvey, T.J.; Wharton, J.A.; Stokes, K.R.; Walsh, F.C.; Wood, R.J.K. A review of experimental techniques to produce a nacre-like structure. *Bioinspir. Biomim.* **2012**, *7*, 031001. [CrossRef] [PubMed]
30. Bidarra, S.J.; Barrias, C.C.; Fonseca, K.B.; Barbosa, M.A.; Soares, R.A.; Granja, P.L. Injectable in situ crosslinkable RGD-modified alginate matrix for endothelial cells delivery. *Biomaterials* **2011**, *32*, 7897–7904. [CrossRef] [PubMed]
31. Ogomi, D.; Serizawa, T.; Akashi, M. Bioinspired organic–inorganic composite materialsprepared by an alternate soaking process as a tissue reconstitution matrix. *J. Biomed. Mater. Res. A* **2003**, *67*, 1360–1366. [CrossRef] [PubMed]
32. Suzawa, Y.; Funaki, T.; Watanabe, J.; Iwai, S.; Yura, Y.; Nakano, T.; Umakoshi, Y.; Akashi, M. Regenerative behavior of biomineral/agarose composite gels as bone grafting materials in rat cranial defects. *J. Biomed. Mater. Res. A* **2010**, *93*, 965–975. [CrossRef] [PubMed]
33. Munro, N.H.; McGrath, K.M. Biomimetic mineralisation of polymeric scaffolds using a combined soaking approach: Adaptation with various mineral salts. *Dalton Trans.* **2011**, *40*, 9269–9275. [CrossRef] [PubMed]
34. Li, H.; Estroff, L.A. Hydrogels coupled with self-assembled monolayers: An in vitro matrix to study calcite biomineralization. *J. Am. Chem. Soc.* **2007**, *129*, 5480–5483. [CrossRef] [PubMed]
35. Helbig, U. Growth of calcium carbonate in polyacrylamide hydrogel: Investigation of the influence of polymer content. *J. Cryst. Growth* **2008**, *310*, 2863–2870. [CrossRef]
36. Sancho-Tomas, M.; Fermani, S.; Goeffredo, S.; Dubinsky, Z.; Garcia-Ruiz, J.M.; Gomez-Morales, J.; Falini, G. Exploring coral biomineralization in gelling environment by means of a counter diffusion system. *CrystEngComm* **2014**, *16*, 1257–1267. [CrossRef]
37. Sancho-Tomas, M.; Fermani, S.; Duran-Olivencia, M.D.; Otalora, F.; Gomez-Morales, J.; Falini, G.; Garcia-Ruiz, J.M. Influence of carged polypeptides on nucleation and growth of $CaCO_3$ evaluated by counterdiffusion experiments. *Cryst. Growth Des.* **2013**, *13*, 3884–3891. [CrossRef]
38. Iijima, M.; Shinozaki, M.; Hatakeyama, T.; Takahashi, M.; Hatakeyama, H. AFM studies on gelation mechanism of xanthan gum hydrogels. *Carbohydr. Polym.* **2007**, *68*, 701–707. [CrossRef]
39. Takahashi, M.; Hatakeyama, T.; Hatakeyama, H. Phenomenological theory describing the behaviour of non-freezing water in structure formation process of polysaccharide aqueous solutions. *Carbohydr. Polym.* **2000**, *41*, 91–95. [CrossRef]
40. Smidsrød, O. Molecular basis for some physical properties of alginates in the gel state. *Faraday Discuss. Chem. Soc.* **1974**, *57*, 263–274. [CrossRef]
41. Huynh, U.T.D.; Lerbret, A.; Neiers, F.; Chambin, O.; Assifaoui, A. Binding of divalent cations to polygalacturonate: A mechanism driven by the hydration water. *J. Phys. Chem. B* **2016**, *120*, 1021–1032. [CrossRef] [PubMed]
42. Leea, K.Y.; Mooneya, D.J. Alginate: Properties and biomedical applications. *Prog. Polym. Sci.* **2012**, *37*, 106–126. [CrossRef] [PubMed]
43. Braissant, O.; Cailleau, G.; Dupraz, C.; Verrecchia, E.P. Bacterially induced mineralization of calcium carbonate in terrestrial environments: The role of exopolysaccarides and amino acids. *J. Sediment. Res.* **2003**, *73*, 485–490. [CrossRef]
44. Kralj, D.; Brečević, L.; Kontrec, J. Vaterite growth and dissolution in aqueous solutions. III. Kinetics of transformation. *J. Cryst. Growth* **1997**, *177*, 248–257. [CrossRef]
45. Yang, X.; Xu, G. The influence of xanthan on the crystallization of calcium carbonate. *J. Cryst. Growth* **2011**, *314*, 231–238. [CrossRef]
46. Li, H.; Estroff, L.A. Calcite growth in hydrogels: Assessing the mechanism of polymer-network incorporation into single crystals. *Adv. Mater.* **2009**, *21*, 470–473. [CrossRef]

47. Butler, M.F.; Glaser, N.; Weaver, A.C.; Kirkland, M.; Heppenstall-Butler, M. Calcium carbonate crystallization in the presence of biopolymers. *Cryst. Growth Des.* **2006**, *6*, 781–794. [CrossRef]
48. Diaz-Dosque, M.; Aranda, P.; Darder, M.; Retuert, J.; Yazdani-Pedrame, M.; Arias, J.L.; Ruiz-Hitzky, E. Use of biopolymers as oriented supports for the stabilization of different polymorphs of biomineralized calcium carbonate with complex shape. *J. Cryst. Growth* **2008**, *310*, 5331–5340. [CrossRef]
49. Flemming, A.A.; Kralj, D. Determination of the composition of calcite-vaterite mixtures by infrared spectrophotometry. *Appl. Spectrosc.* **1991**, *45*, 1748–1751.
50. Fleming, A.A.; Brecevic, L. Infrared spectra of amorphous and crystalline calcium carbonate. *Acta Chem. Scand.* **1991**, *45*, 1018–1024.
51. Kontrec, J.; Ukrainczyk, M.; Babic-Ivancic, V.; Kralj, D. Synthesis of calcium carbonate by semicontinuous carbonation method in the presence of dextrans. *Croat. Chem. Acta* **2011**, *84*, 25–32. [CrossRef]
52. Kralj, D.; Kontrec, J.; Brecevic, L.; Falini, G.; Nothing-Laslo, V. Effect of inorganic anions on the Morphology and structure of magnesium calcite. *Chem. Eur. J.* **2004**, *10*, 1647–1656. [CrossRef] [PubMed]
53. Raz, S.; Hamilton, P.S.; Wilt, F.H.; Weiner, S.; Addadi, L. The transient phase of amorphous calcium carbonate in sea urchin larval spicules: The involvement of proteins and magnesium ions in its formation and stabilization. *Adv. Funct. Mater.* **2003**, *13*, 480–486. [CrossRef]
54. Beniash, E.; Aizenberg, J.; Addadi, L.; Weiner, S. Amorphous calcium carbonate transforms into calcite during sea urchin larval spicule growth. *Proc. R. Soc. Lond. B* **1997**, *264*, 461–465. [CrossRef]
55. International Centre for Diffraction Data. *Powder Diffraction File, Inorganic Volume*; Table Nos. 88-1087, 86-0174, 83-0578 for Calcilte; 33-0268 for Vaterite; International Centre for Diffraction Data: Swarthmore, PA, USA, 1988.
56. Plummer, L.N.; Busenberg, E. The solubilities of calcite, aragonite and vaterite in CO_2-H_2O solutions between 0 and 90 °C, and an evaluation of the aqueous model for the system $CaCO_3$-CO_2-H_2O. *Geochim. Cosmochim. Acta* **1982**, *46*, 1011–1040. [CrossRef]
57. Kralj, D.; Brecevic, L.; Nielsen, A.E. Vaterite growth and dissolution in aqueous solutions. I. Kinetics of crystal growth. *J. Cryst. Growth* **1990**, *104*, 793–800. [CrossRef]